Virology 404 (2010) 78–88

Contents lists available at ScienceDirect

Virology

journal homepage: www.elsevier.com/locate/yviro

Characterization of the antiviral and inflammatory responses against Nipah virus in endothelial cells and neurons ☆

Michael K. Lo [a,b,*], David Miller [c], Mohammad Aljofan [d], Bruce A. Mungall [d], Pierre E. Rollin [c], William J. Bellini [a], Paul A. Rota [a]

[a] Measles, Mumps, Rubella, and Herpesvirus Laboratory Branch, Centers for Disease Control and Prevention, Mailstop C-22, 1600 Clifton Road, Atlanta, GA 30333, USA
[b] Emory University, Laney Graduate School, Graduate Division of Biological and Biomedical Sciences, Immunology and Molecular Pathogenesis Program, 1462 Clifton Road Suite 314, Atlanta, GA 30322, USA
[c] Special Pathogens Branch, Centers for Disease Control and Prevention, 1600 Clifton Road, Atlanta, GA 30333, USA
[d] Australian Animal Health Laboratory, Commonwealth Scientific and Industrial Research Organization, 5 Portarlington Road, Geelong, Victoria 3220, Australia

ARTICLE INFO

Article history:
Received 12 March 2010
Returned to author for revision
30 March 2010
Accepted 3 May 2010
Available online 23 May 2010

Keywords:
Nipah
Endothelial
Neuronal
Chemokines
Interferon
W protein
Pathogenesis

ABSTRACT

Nipah virus (NiV) is a highly pathogenic paramyxovirus which causes fatal encephalitis in up to 75% of infected humans. Endothelial cells and neurons are important cellular targets in the pathogenesis of this disease. In this study, viral replication and the innate immune responses to NiV in these cell types were measured. NiV infected endothelial cells generated a functionally robust IFN-β response, which correlated with localization of the NiV W protein to the cytoplasm. There was no antiviral response detected in infected neuronal cells. NiV infection of endothelial cells induced a significant increase in secreted inflammatory chemokines, which corresponded with the increased ability of infected cell supernatants to induce monocyte and T-lymphocyte chemotaxis. These results suggest that pro-inflammatory chemokines produced by NiV infected primary endothelial cells *in vitro* is consistent with the prominent vasculitis observed in infections, and provide initial molecular insights into the pathogenesis of NiV in physiologically relevant cells types.

Published by Elsevier Inc.

Introduction

Nipah virus (NiV) is a highly pathogenic member of the family *Paramyxoviridae*, in the subfamily *Paramyxovirinae*, in which it along with Hendra virus makes up the genus *Henipavirus* (Mayo, 2002). The ability to generate multiple proteins from a single phosphoprotein (P) gene by mRNA editing, and/or use of alternative open reading frames is common among paramyxoviruses (Curran and Kolakofsky, 1990; Giorgi et al., 1983; Kolakofsky et al., 2005; Liston and Briedis, 1995). These accessory proteins typically have the ability to antagonize the host's innate immune response (Gotoh et al., 2002; Horvath, 2004). Expression of the NiV C, V, and W proteins from plasmid DNA indicated their varying abilities to antagonize the innate antiviral response in avian and human cell lines. The NiV C, V, and W proteins were able to rescue the replication of an interferon (IFN) sensitive Newcastle Disease virus (Park et al., 2003). The N-terminal region shared by the NiV P, V, and W proteins binds to signal transduction activator of transcription (STAT)-1, thus preventing its activation by phosphorylation (Rodriguez et al., 2004, 2002; Shaw et al., 2004). The nuclear localization of the NiV W protein enhanced its ability to antagonize the activation of interferon regulatory factor (IRF) 3 (Shaw et al., 2005). Characterization of these proteins in NiV infected cells showed that the phosphoprotein (P) gene mRNA of NiV is edited at a high frequency to yield mRNAs coding for the NiV V and W proteins, and that an alternative reading frame in the P gene is utilized to generate the C protein (Kulkarni et al., 2009; Lo et al., 2009). NiV C and V were localized to the cell cytoplasm, while NiV W was detected in the nucleus, and all of the proteins were detected in preparations of purified virions (Lo et al., 2009). The interaction between plasmid-expressed NiV W and karyopherin α3/4 (KPNA3/4) was also detected in NiV infected cells (Lo et al., 2009; Shaw et al., 2005). More recently, a reverse genetic study indicated a crucial role of the NiV C protein in viral replication, and showed that phosphorylated STAT-1 was precluded from translocating into the nuclei of wild-type NiV infected Vero E6 cells, while a STAT-1 binding mutant virus allowed for its nuclear translocation (Ciancanelli et al., 2009). The results of these studies lead to the question as to whether NiV infection of physiologically relevant target cells produces similar results as those seen in the standard cell lines used for viral propagation.

☆ Disclaimer: The findings and conclusions in this report are those of the authors and do not necessarily represent the views of the Centers for Disease Control and Prevention.

* Corresponding author. 1600 Clifton Road, Mailstop C-22, Atlanta, GA 30333, USA. Fax: +1 404 639 4187.
E-mail address: mko2@cdc.gov (M.K. Lo).

0042-6822/$ – see front matter. Published by Elsevier Inc.
doi:10.1016/j.virol.2010.05.005

NiV causes severe encephalitis in humans, characterized by systemic vasculitis and necrosis particularly in the central nervous system (CNS). Extensive infection of neurons, endothelial cells, and smooth muscle cells of blood vessels is characteristic of human NiV infections (Wong et al., 2002). The molecular basis of NiV pathogenesis is still unclear. The inflammatory cellular infiltrate found in the central nervous system (CNS) during NiV encephalitis includes neutrophils, macrophages, lymphocytes, and reactive microglia (Wong et al., 2002). The recruitment of these cells indicates the possible action of small molecule messengers and chemoattractants known as cytokines and chemokines. Some inflammatory cytokines found in infectious CNS pathology include TNFα and IL-6, while some chemokines include IL-8 (CXCL8), RANTES (CCL5), MIP-1α (CCL3), MCP-1 (CCL2), and IP-10 (CXCL10) (Glabinski and Ransohoff, 1999). The cellular sources of these secreted cytokines are varied, as cells of the CNS as well as the inflammatory infiltrate have the ability to produce and secrete these molecules (Griffin, 1997; Owens et al., 2005). These cytokines and chemokines are also produced in response to pulmonary inflammation due to infection with mycobacterium and respiratory syncytial virus (RSV) (Kunkel et al., 2002; Pace et al., 1999; Penido et al., 2003). In order to address the physiological relevance of previous studies performed in Vero cells, we characterized and compared the growth characteristics of NiV in several primary human endothelial cells and a human neuroblastoma cell line. Our findings indicate a significant difference in viral replication rate between neurons and endothelial cells. This difference corresponded to the ability of endothelial cells to generate an IFN-β response, which correlated with a differential subcellular localization of NiV W between endothelial cells and neurons. We also demonstrated a significant increase of inflammatory chemokines present in supernatants of NiV infected cells, and showed that increases in these chemokines correlated with increased induction of functional monocyte and T-lymphocyte chemotaxis.

Results

The rate of NiV replication is significantly higher in neuronal cells than in endothelial cells

In order to measure and compare the infectivity of human endothelial and neuronal cells, a chemiluminescent immunolabeling assay was performed in which levels of NiV nucleoprotein (N) served as an indicator of viral replication (Aljofan et al., 2008). Significant levels of NiV antigen could not be detected in the EA926.hy HUVEC-A549 fusion hybrid cells, which served as a negative control (Erbar et al., 2008). At 16 h post-infection, the primary human umbilical cord vein endothelial cells (HUVEC), human lung microvascular endothelial cells (HULEC), and immortalized human endothelial brain cells (HBEC) were infected with NiV, while the levels of NiV N detected in the M17 neuronal cells were at least twice the levels found in any of the endothelial cells used in this assay (Fig. 1). To determine whether this disparity in NiV N protein expression levels was due to a difference in the rate of viral replication between cell lines, a single-step growth curve was performed for human lymphatic lung microvascular endothelial cells (LYMEC), HUVEC, HULEC, HBEC, and M17 cells (Fig. 2A). At 16 h post-infection (MOI = 1), the viral titer in M17 cells reached ~10^7 $TCID_{50}$/mL, which indicated a high rate of

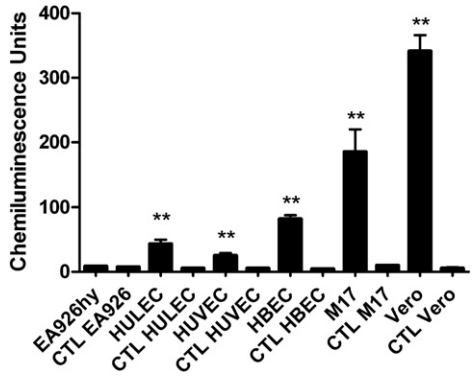

Fig. 1. Levels of NiV antigen produced by neuronal cells are greater than those produced by endothelial cells. In this immunolabeling assay, endothelial and neuronal cells were infected for 16 h, then fixed, washed, and incubated with rabbit anti-NiV N antibodies. A mouse anti-rabbit IgG antibody conjugated with horseradish peroxidase was used as a means to measure relative levels of NiV antigen. CTL indicates uninfected controls for each respective cell type. ** ($P<0.001$) (two-tailed Student's *t*-test with Welch's modification) Compared to levels of chemiluminescence detected from respective mock-infected endothelial/neuronal cell types. Error bars indicate one standard deviation of the mean of 5 replicates.

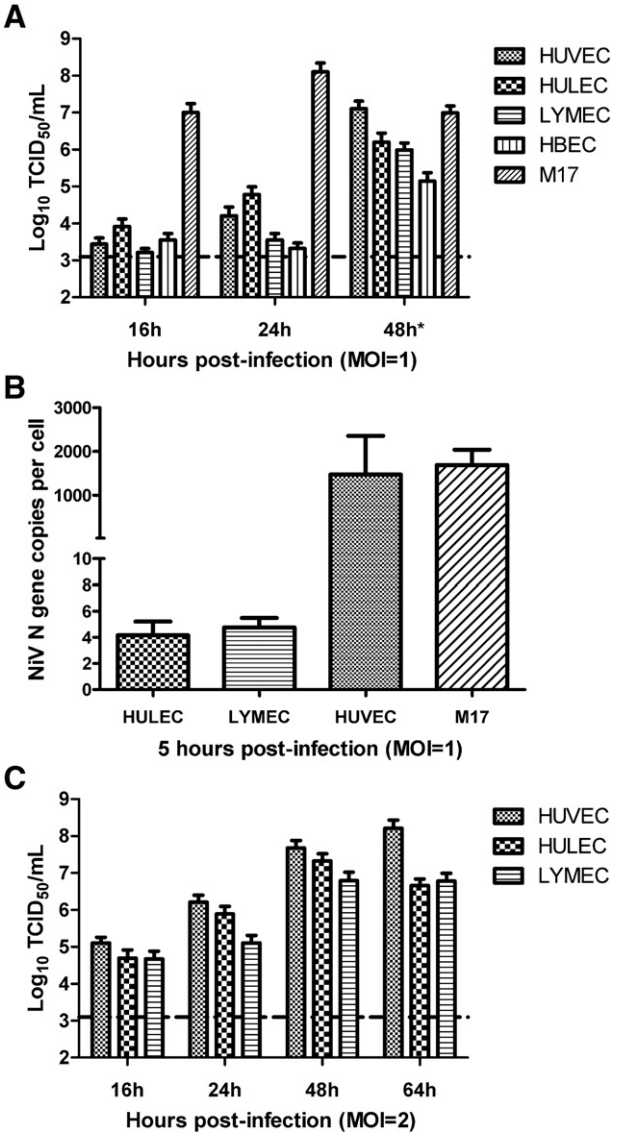

Fig. 2. Differential susceptibility and growth rate of NiV in endothelial and neuronal cells. A) Supernatants taken from NiV infected endothelial cells and neuronal cells (infected at MOI = 1) were serially diluted before being used to infect Vero cells to determine the $TCID_{50}$/mL at the indicated time points. (* supernatant from M17 was taken from a 32 h time point) B) The levels of NiV genome were measured from NiV infected (MOI = 1) endothelial and neuronal cell lysates after 5 h of infection to determine the relative infectibility of infection of each cell type. C) NiV infection of HUVECs and HULECs (MOI = 2). The dotted line delineates the limit of detection (3.1). Error bars indicate one standard deviation of the mean of 9 replicates for the growth curve experiments (A and C), and of 3 replicates of the genome copy number experiment (B).

viral replication. Peak viral titers were achieved in infected M17 cells by 24 h post-infection; the drop in viral titer at 32 h post-infection was likely due to both the lack of cells remaining to infect as well as to viral degradation. In contrast, for the endothelial cells infected with NiV, the viral titer was barely above the lower limit of detection by 16 h post-infection, though higher titers were detected at 48 h (Fig. 2A). The delay in viral antigen production and viral titer increase by the endothelial cells relative to the neuronal cells (Fig. 1) could be due to differences in the ability of NiV to infect these cell types. In order to determine potential differences in susceptibility to NiV infection between the cell types, we extracted total RNA from infected cells (MOI = 1) at 5 h post-infection and used real-time PCR to determine the relative number of N gene copies present per cell. We detected high copy numbers of NiV N gene in NiV infected HUVECs and M17 neuronal cells (~1400–1700 copies per cell), and substantially lower copy numbers in HULECs and LYMECs (~4–5 copies per cell) (Fig. 2B).

To ensure that a majority of endothelial cells were being infected, we repeated the growth curve experiment in HUVECs, HULECs, and LYMECS but increased the MOI to 2. By increasing the input virus, there was a substantial increase of approximately 1.5 logs in viral titer in the three endothelial cell types at 16 h post-infection (Fig. 2C). Nevertheless, the rate of replication still did not reach that of NiV in M17 cells, which yielded 100-fold higher viral titer at the same time point (Fig. 2A). Notably, in spite of the significant increase in titer at 16 h post-infection in endothelial cell infection provided by increasing the MOI, there was only a modest (3-fold) difference in titer by 48 h post-infection between cells infected at a MOI of one versus two.

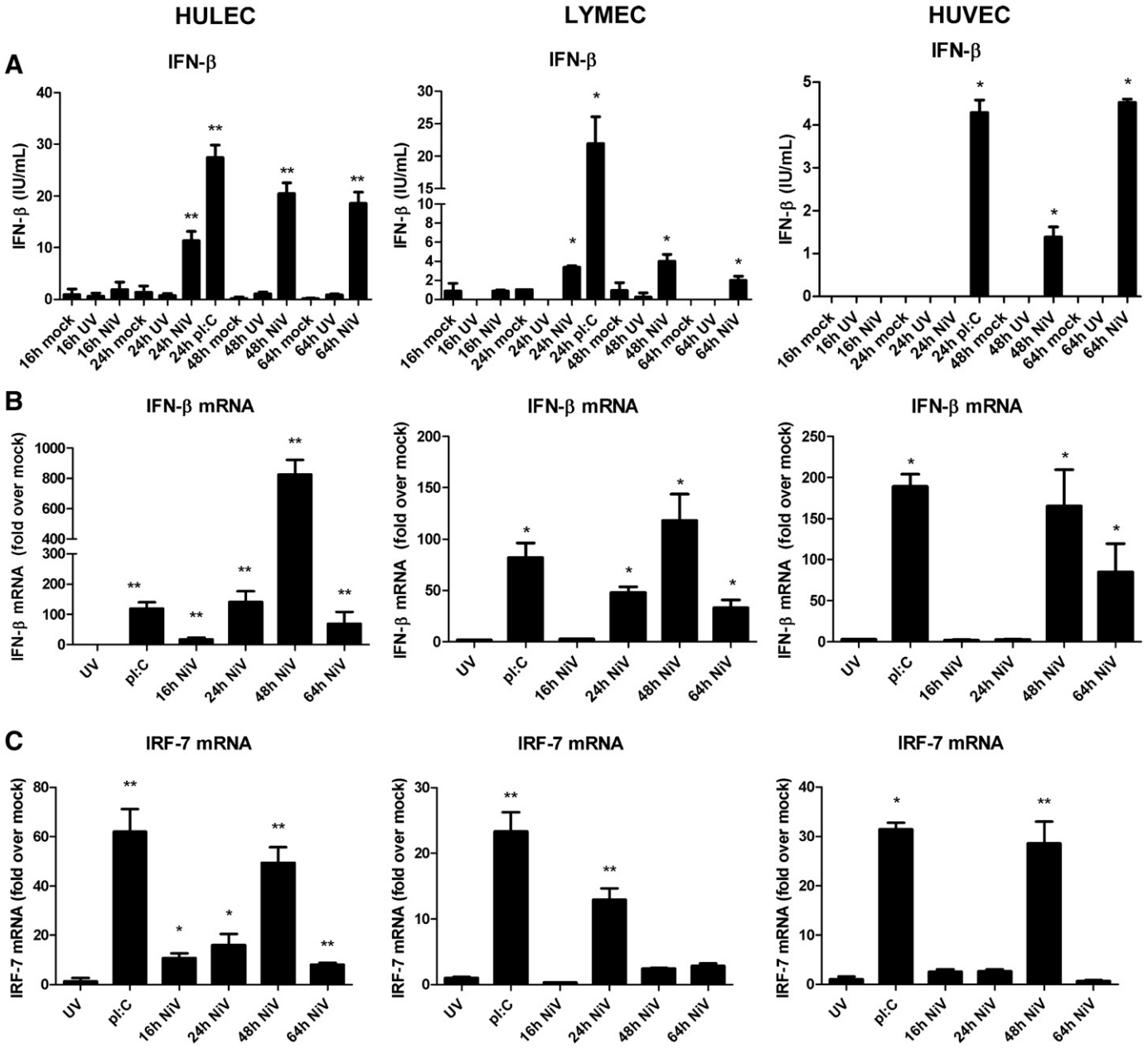

Fig. 3. NiV infection of endothelial cells induces IFN-β production. A) IFN-β ELISA was performed on supernatants taken from NiV infected lung, lymphatic, and umbilical vein endothelial cells at indicated time points. B) Levels of IFN-β mRNA and C) IF-7 mRNA transcription in NiV infected lung, lymphatic, and umbilical vein endothelial cells were measured by Real-time PCR, which was performed on cDNA generated from extracted total cellular RNA using oligo-dT_{12-18} primers. Error bars denote one standard deviation from the mean of 3 replicates. Labels above the graphs correspond to the data obtained from each endothelial cell type. *($P<0.05$); **($P<0.01$) (two-tailed Student's *t*-test with Welch's modification) A: Relative to levels of IFN-β detected in supernatants from mock-infected cells at corresponding time point; B and C: Relative to mRNA transcript levels in mock-infected cells at corresponding time point.

While the lower NiV endpoint titers from infected HULECs and LYMECs may be due to lower levels of infectibility (Figs. 2A, C), the observation that the HUVECs supported NiV replication to a similar titer as the M17 cells but reached that titer later in infection, (64 h post-infection) suggests that innate cellular response mechanisms in endothelial cells may limit early viral replication (Fig. 2C).

NiV infected endothelial cells produce a functional antiviral response

In order to determine the presence or absence of an innate antiviral response to NiV infection, we performed IFN-β ELISA on gamma-irradiated supernatants collected from infected cells. While we confirmed the ability of M17 cells to produce functional IFN-β (Supplemental Figure 1D), we did not detect an increase in levels of IFN-β from NiV infected M17 cell supernatants relative to mock-infected cell controls (data not shown). We detected IFN-β in supernatants from endothelial cells above baseline levels as early as 16 h post-infection (Fig. 3A, HULEC). The HULECs produced the highest levels of IFN-β in response to NiV infection. The LYMECs also generated IFN-β in response to NiV infection with a similar time course, but produced lower peak levels of IFN-β compared to HULECs. The HUVECs had a slightly delayed IFN-β response compared with the HULECs and LYMECs, and also produced 5-fold lower levels of IFN-β than the other two endothelial cell types (Fig. 3A). The increases in IFN-β mRNA transcripts of the infected endothelial cells generally corresponded to the time points in which increased levels of these proteins in the supernatants were observed (Fig. 3B). For positive controls, each endothelial cell type was treated with 50 μg/mL of poly-I:C for 24 h before the supernatant was harvested to be assayed for IFN-β. The capacity to produce IFN-β varied according to the particular endothelial cell type. Both the lung-derived HULECs and LYMECs produced 20–25 IU/mL of IFN-β when stimulated with poly-I:C, while HUVECs only produced approximately 4 IU/mL of IFN-β. We observed that the induction of IFN-β in the infected endothelial cells required viral replication, as UV inactivated virus failed to induce the endothelial cells to produce significant levels of IFN-β (Fig. 3A). We also measured IRF-7 mRNA levels at the same time points to determine whether IFN-β signaling was occurring in infected cells (Fig. 3C). Our results indicated that IRF-7 mRNA levels in each endothelial cell type were upregulated at time points which corresponded with those in which IFN-β was detected in culture supernatants. (Fig. 3C). For HULECs, we found that at 16 and 24 h post-infection, the IRF-7 mRNA levels were approximately 10 fold higher than those of mock-infected cells., At 48 h, these levels had increased to 50 fold relative to mock-infected cell; and then decreased to baseline levels by 64 h. In LYMECs, IRF-7 mRNA was upregulated at 24 h (~15 fold), only to drop off by 48 h (Fig. 3C), which may indicate that signaling in LYMECs may be inhibited at later time points. In HUVECs, IRF-7 mRNA was upregulated at 48 h, which corresponded to the presence of IFN-β in culture supernatants at that time point, and see a drop off at 64 h post-infection. For all 3 endothelial cell types, there was a period of time following upregulation of IFN-β in which IRF-7 mRNA levels significantly increased, which indicates that at least during those time points, type-I IFN signaling was not inhibited.

To determine whether the IFN-β produced from NiV infected endothelial cells was functional, we performed an biologic assay to measure the ability of the supernatants to protect cells from the cytopathic effect (CPE) caused by encephalomyocarditis virus (EMCV). Pre-treatment of A549 human lung airway epithelial cells with gamma-irradiated supernatants from NiV infected HULECs and LYMECs at 24, 48, and 64 h provided significant protection of the cells from EMCV-induced CPE, with HULEC supernatants providing some protection even at 16 h (Figs. 4A and B). Supernatants from NiV infected LYMECs at 24 h showed 2-fold less protection than the protection from the corresponding time point from HULEC supernatants. In correlation with the comparatively lower levels of IFN-β produced by HUVECs, pre-treatment of A549 cells with NiV infected HUVEC supernatants provided some protection from EMCV CPE, but the level of protection was not as high as that provided by NiV infected HULEC and LYMEC supernatants (Fig. 4C).

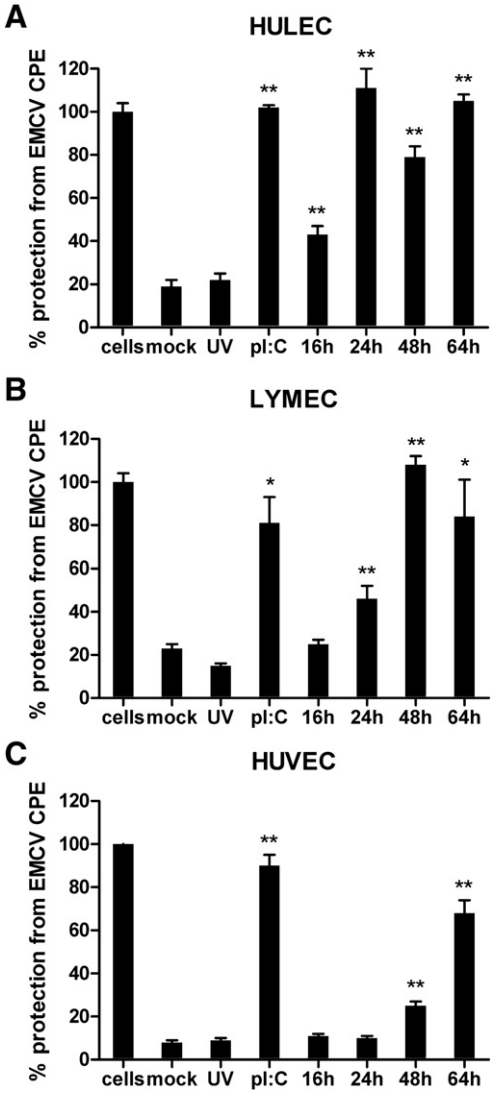

Fig. 4. Supernatants from NiV infected endothelial cells contain functional IFN-β. A549 human respiratory epithelial cells were pre-treated with gamma-irradiated supernatants from mock, UV inactivated NiV, or NiV infected HULECs (panel A), LYMECs (panel B), or HUVECs (panel C) for 6 h, and then infected with ~200 PFU/well EMCV for 16–20 h. Cells were stained with crystal violet and absorbance at 600 nm was measured. Error bars indicate one standard deviation from the mean of 3 replicates. **($P<0.01$); *($P<0.05$) (two-tailed Student's *t*-test with Welch's modification) Relative to cells treated with supernatants from mock-infected cells at corresponding time points.

Cell-type specific subcellular localization of NiV W

We have shown previously that the accessory proteins (NiV C, V, and W proteins) derived from the NiV P gene have distinct subcellular localizations in infected Vero cells (Lo et al., 2009). We performed immunofluorescence assays on the NiV infected neuronal and endothelial cells to determine whether these proteins localized to similar compartments as in Vero cells. Interestingly, we found that while the NiV W localized to the nucleus of M17 cells as it did in Vero cells, it was primarily found in the cytoplasm of all endothelial cell types that we infected with NiV (Fig. 5). When expressed from

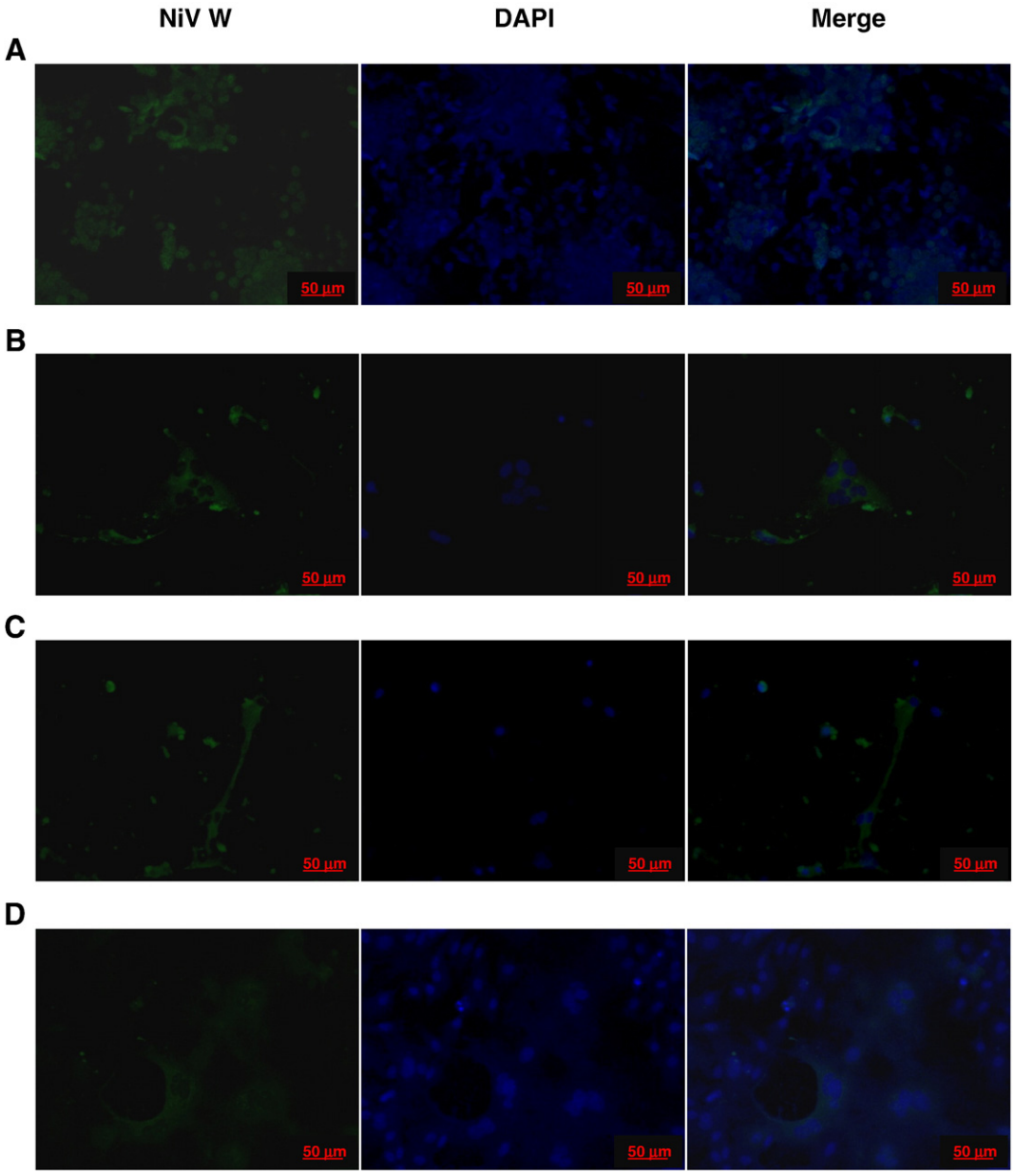

Fig. 5. Differential subcellular localization of NiV W protein in NiV infected neuronal and endothelial cells. NiV W was detected in infected A) M17 neuronal cells, B) HULEC, C) LYMEC, and D) HUVEC. Staining for NiV W is in the left-most column using FITC, nuclear staining is in the middle column using DAPI, and a merged image of the two is shown in the right-most column. Magnification: 20×.

plasmid DNA, the NiV V and W proteins have antagonistic activities for IFN-β promoter activation caused by Sendai virus infection. The nuclear localization of plasmid-expressed NiV W allows it to block both TLR-3 and virus-induced IFN-β induction pathways (Shaw et al., 2005). Our finding that the majority of NiV W protein produced during infection of endothelial cells is excluded from the nucleus suggest that TLR-3 mediated induction of IFN-β expression is not inhibited in endothelial cells as they produce IFN-β during NiV infection.

NiV infection induces production of inflammatory chemokines and promotes monocyte and T-lymphocyte chemotaxis

One of the main pathological findings from humans infected with NiV is vasculitis characterized by focal and transmural mixed inflammatory infiltrates consisting of neutrophils, macrophages, lymphocytes, and microglia (Wong et al., 2002). Since endothelial cells are one of the primary targets of NiV infection, we wanted to determine whether endothelial cells could serve as a source of

Fig. 6. NiV infection induces production of inflammatory chemokines associated with increased monocyte chemotaxis in endothelial cells. A and C) Luminex bead assays were performed on gamma-irradiated NiV infected HULEC and LYMEC supernatants to detect the presence of IL-8 and MCP-1. B and D) Levels of IL-8 and MCP-1 mRNA transcription in NiV infected HULEC and LYMEC were measured by real-time PCR, which was performed using cDNA generated from extracted total cellular RNA using oligo-dT_{12-18} primers. (E) THP-1 monocyte chemotaxis assay. Levels of THP-1 monocytic cell chemotaxis across a 5 μm pore membrane induced after 2 h of exposure to above mentioned supernatants relative to levels of chemotaxis induced by supernatants from poly-I:C stimulated endothelial cells. Labels above the graphs correspond to the data obtained from each endothelial cell type. Error bars indicate one standard deviation of the mean of 3 replicates. $^{**}(P<0.01)$, $^{*}(P<0.05)$. (two-tailed Student's *t*-test with Welch's modification) A, C: Compared to chemokine levels in mock treated supernatants at corresponding time point; B, D: Compared to levels of mRNA from mock-infected endothelial cells at corresponding time point; E: Compared to levels of chemotaxis induced by mock treated endothelial cell supernatants at corresponding time point.

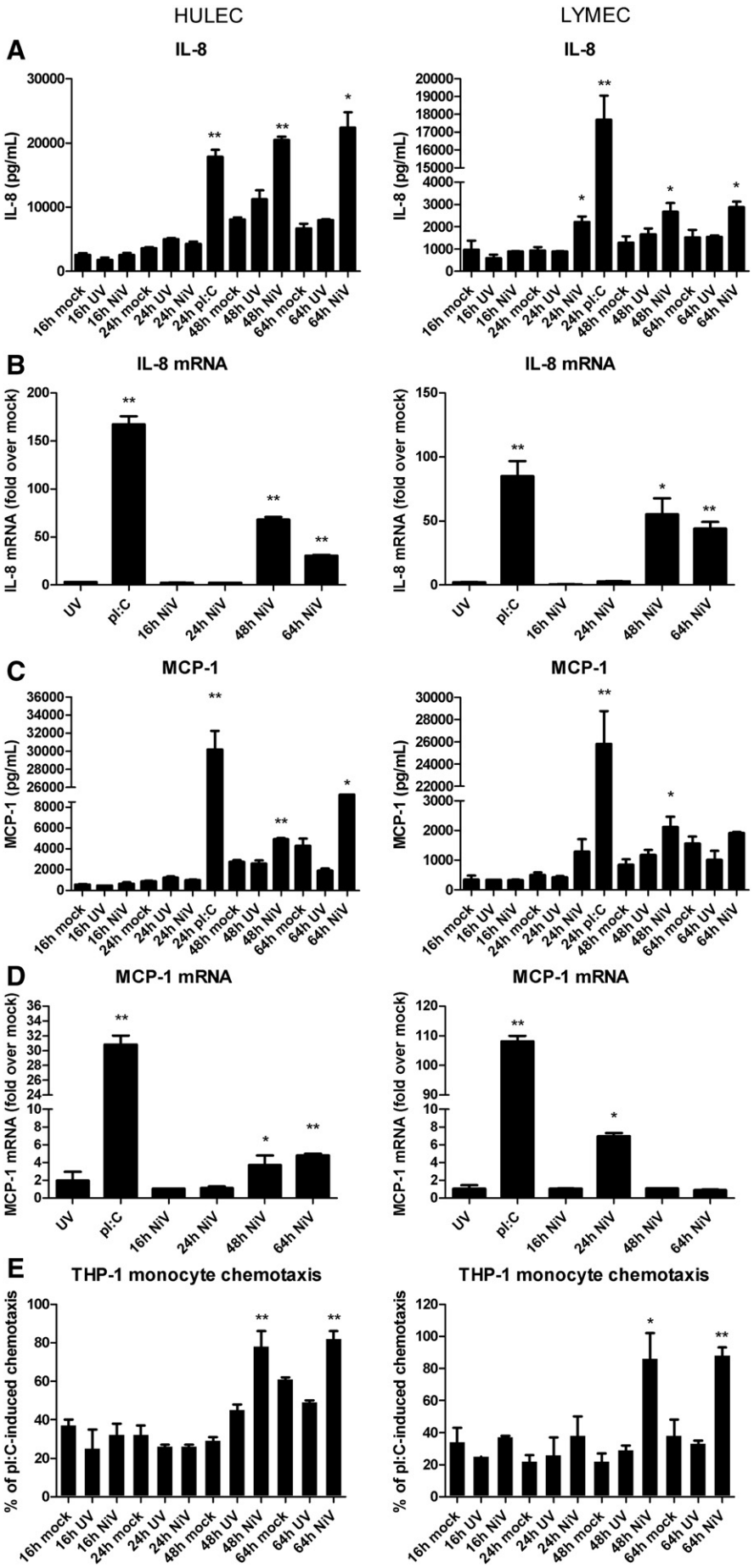
HULEC
LYMEC
A
IL-8
IL-8 (pg/mL)
B
IL-8 mRNA
IL-8 mRNA (fold over mock)
C
MCP-1
MCP-1 (pg/mL)
D
MCP-1 mRNA
MCP-1 mRNA (fold over mock)
E
THP-1 monocyte chemotaxis
% of pI:C-induced chemotaxis
16h mock
16h UV
16h NiV
24h mock
24h UV
24h NiV
24h pI:C
48h mock
48h UV
48h NiV
64h mock
64h UV
64h NiV
UV
pI:C
16h NiV
24h NiV
48h NiV
64h NiV

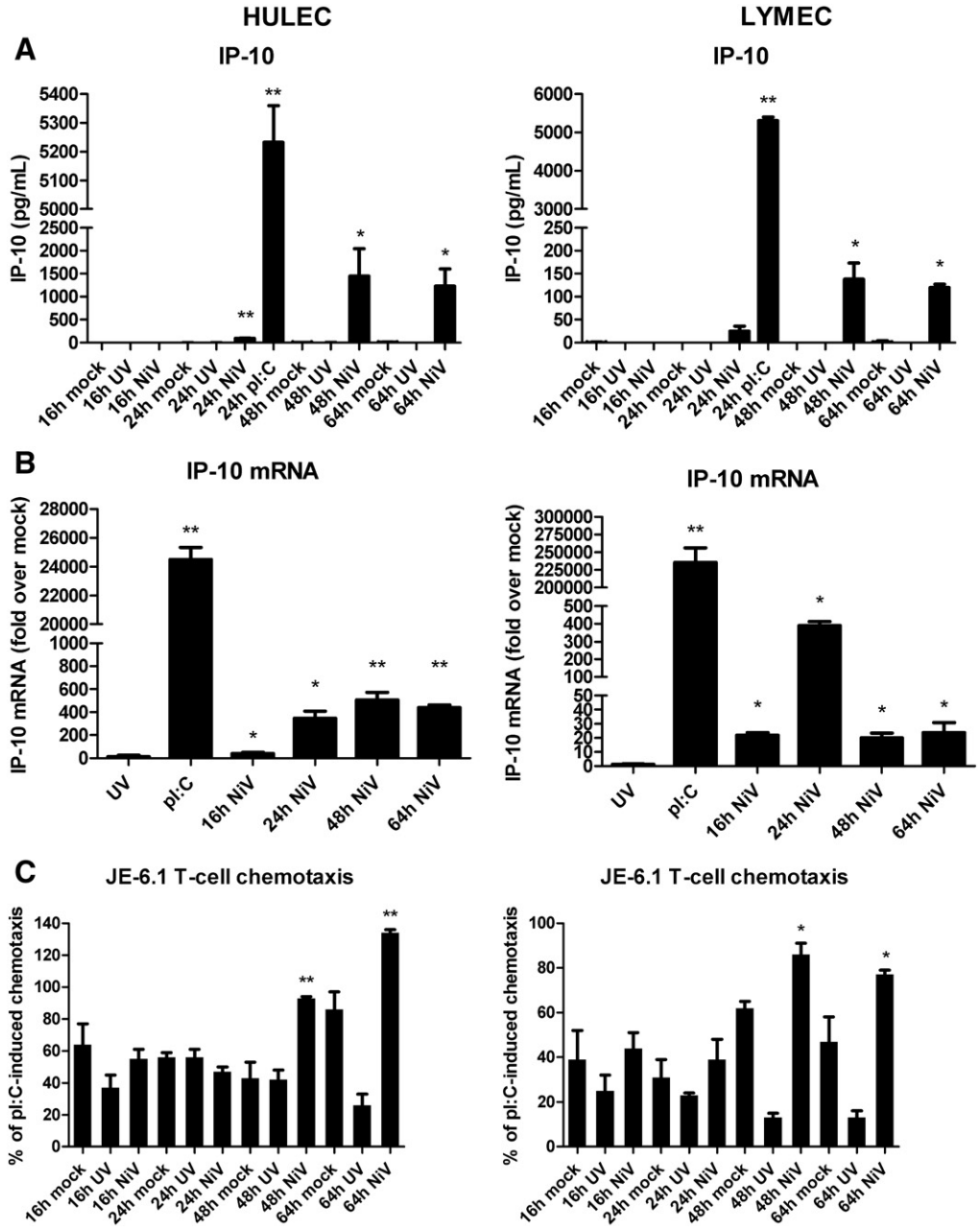

Fig. 7. NiV infection induces production of inflammatory cytokines associated with increased T-lymphocyte chemotaxis in endothelial cells. A) Luminex bead assays were performed on gamma-irradiated NiV infected HULEC and LYMEC supernatants to detect the presence of IP-10 (CXCL10). B) Levels of IP-10 mRNA transcription in NiV infected HULEC and LYMEC were measured by real-time PCR, which was performed using cDNA generated from extracted total cellular RNA using oligo-dT_{12-18} primers. C) Levels of JE-6.1 T-lymphocyte chemotaxis across a 5 μm pore membrane induced after 2 h of exposure to NiV infected HULEC and LYMEC supernatants relative to supernatants from poly-I:C stimulated endothelial cells. Labels above the graphs correspond to the data obtained from each endothelial cell type. Error bars indicate one standard deviation of the mean of 3 replicates. **($P<0.01$), *($P<0.05$). (two-tailed Student's *t*-test with Welch's modification) A: Compared to mock-infected endothelial cell supernatants at corresponding time point; B: Compared to mock-infected endothelial cell mRNA transcript levels at corresponding time point; C: Compared to chemotaxis induced by mock supernatants at corresponding time point.

inflammatory cytokines and chemokines that would contribute to the manifestation of vasculitis seen in human disease. Luminex multiplex bead array assays were performed to detect the presence of inflammatory cytokines and chemokines in NiV infected HULEC and LYMEC supernatants. In spite of a gradual increase in levels of MCP-1 and IL-8 in mock treated endothelial cell supernatants due to accumulated basal levels of expression of both chemokines over time, we detected significant increases above baseline levels of IL-8, MCP-1, IP-10, and IL-6 (IL-6 upregulation only in HULECs — data not shown) consistently by 48 h post-infection (Figs. 6A, C; Fig. 7A). We did not find significant increases in these chemokines in HUVEC or M17 cell supernatants (data not shown). We demonstrated that viral replication was required in order to induce upregulated levels of these chemokines, as UV inactivated virus stocks did not significantly increase levels of these chemokines at any of the corresponding time points in which we harvested supernatants (Figs. 6A, C; Fig. 7A). The substantial increases (from 4 fold to 60-fold) we observed in mRNA transcription of these genes over baseline levels generally corresponded to the time points in which increased levels of these proteins in the supernatants was observed (Figs. 6B, D; Fig. 7B). In order to determine any functional significance correlated with these upregulated chemokines, we performed chemotaxis assays using the THP-1 monocyte and the JE-6.1 T-lymphocyte cell lines. We observed that the supernatants taken from NiV infected HULEC and LYMECs at 48

and 64 h post-infection induced a significant increase in both monocyte and lymphocyte chemotaxis over mock supernatants (Figs. 6E, 7C). Supernatants taken from poly-I:C stimulated endothelial cells consistently induced high levels of chemotaxis, and were used as the positive control representing maximum induction of chemotaxis.

Discussion

This is the first report characterizing the innate antiviral responses of human primary endothelial cells against NiV infection. Despite previous reports of the ability of NiV V and W proteins to block IFN-β production via TLR-3 and mda-5 mediated signaling (Parisien et al., 2009; Shaw et al., 2005), we have shown that NiV infected primary human endothelial cells can generate a functional IFN-β response. Surprisingly, we found that the majority of NiV W protein detected by immunofluorescence assays of NiV infected endothelial cells localized to the cytoplasm, contrary to the nuclear localization in infected M17 neuronal cells as shown in this study, and in infected Vero and plasmid transfected HeLa cells as shown in prior studies (Lo et al., 2009; Shaw et al., 2005). Since nuclear localization of plasmid-expressed NiV W was required to block TLR-3 signaling by over expression of TRIF, it is possible that TLR-3 signaling is the means by which primary endothelial cells generate the observed IFN-β response to NiV infection. Another possibility regarding the source of IFN-β production is via the RIG-I RNA helicase pathway. RIG-I is responsible for inducing cytokine responses to the stem loop structured leader of measles virus, as well as to Sendai virus infection (Melchjorsen et al., 2005; Plumet et al., 2007; Shingai et al., 2007). Parainfluenza simian virus 5 (PIV5) has a genomic promoter sequence that limits detection by RIG-I (Manuse and Parks, 2009). While many paramyxovirus V proteins, including that of NiV, bind and inhibit the antiviral signaling activity of mda-5, they have not had the same effect on RIG-I (Childs et al., 2007, 2009; Parisien et al., 2009). It is possible that in spite of the ability of NiV infected endothelial cells to mount an IFN-β response as early as 16 h post-infection, NiV is able to overcome the effects of IFN-β signaling, because we detected a continual increase in virus titer in the presence of IFN-β production (Figs. 2 and 3). We did not detect any evidence of IFN-β expression at earlier time points of endothelial cell infection (2, 5, and 8 h) (Supplemental Figures 1A–C, 2). Given the ability of the NiV V and W proteins to inhibit the induction of IFN-β, a reverse genetic approach would be warranted to study the potential actions of these proteins at early time points (Childs et al., 2007; Shaw et al., 2005). While we have measured IRF7 mRNA levels in this study (Fig. 3C), it is worth investigating the cellular localization of phosphorylated/unphosphorylated Interferon Regulatory Factors 3 and 7 (IRF-3 and IRF-7) in endothelial cells to evaluate additional mechanisms that provide avenues for type-I IFN production. The results obtained from the immunofluorescence assays of NiV W protein in this study highlight the benefits of utilizing primary endothelial cells in attempting to study the pathogenesis of NiV infection, as they significantly differ from infections performed in both IFN-incompetent and competent cell lines (Vero, Vero E6, 293T) (Ciancanelli et al., 2009; Emeny and Morgan, 1979; Lo et al., 2009).

While the macroscopic pathological features of NiV infection in humans have been well described (Wong et al., 2002), the molecular mechanisms underlying the pathogenesis of NiV infection remain largely undefined. Given the pronounced vasculitis observed in the CNS and lungs of human cases, we hypothesized that measuring the presence of inflammatory chemokines secreted by primary targets of NiV infection would identify possible mechanisms by which the observed vasculitis is induced. Chemokines play a major role in guiding the migration of cells, and are a diverse family of low molecular weight proteins that are divided into 4 subfamilies based on structure and function. Two major subfamilies include the CXC and CC chemokines. CXC chemokines are split into two types, those that contain a glutamate-leucine-arginine (ELR) motif, and those that do not (non-ELR). CXC chemokines that have the ELR motif (i.e., IL-8/CXCL8) primarily attract neutrophils and are associated with bacterial infections, but have limited effects on T cells and monocytes. Non-ELR CXC chemokines (i.e., IP-10/CXCL10) tend to attract activated T cells and NK cells, and are typically associated with antiviral activities (Mahalingam et al., 1999). On the other hand, CC chemokines (i.e., MCP-1/CCL2) attract T cells, monocytes, and macrophages, but not neutrophils (Lane et al., 2006). We have shown that NiV infection of human lung and lung lymphatic endothelial cells results in the upregulation of inflammatory chemokines MCP-1, IL-8, and IP-10 which may contribute to the induction of both monocyte and T-lymphocyte chemotaxis. In clinical settings, epyema and parapneumonic effusions are associated with upregulated levels of MCP-1 and IL-8 that functionally induce chemotaxis (Antony et al., 1993). A cDNA array study of respiratory syncytial virus (RSV) infection of human airway epithelial cells indicated an increase in IL-8 and MCP-1, which correlates with observed peribronchial mononuclear infiltrate, with eosinophilic and basophilic degranulation in human infections (Zhang et al., 2001). Alveolar hemorrhage, pulmonary edema, and aspiration pneumonia were seen in the initial NiV outbreak, as well as in subsequent Bangladesh outbreaks, in which an increase in the rate of severe respiratory distress was reported (Goh et al., 2000; Hossain et al., 2008; Lee et al., 1999; Paton et al., 1999; Wong et al., 2002). Importantly, MCP-1, IL-8, and IP-10 are upregulated in both experimental infectious and non-infectious CNS pathology in monkeys, mice and rats (Glabinski and Ransohoff, 1999). All three chemokines play a role in lymphocyte trafficking in CNS diseases (Klein, 2004; Loetscher et al., 1994; Pace et al., 1999; Penido et al., 2003). MCP-1 also regulates permeability of the blood–brain–barrier through altering the arrangement of endothelial tight junction proteins (Stamatovic et al., 2005). Clinical studies of patients infected with Japanese encephalitis virus showed that infection is correlated with elevated levels of IL-8 in the cerebrospinal fluid (CSF) (Singh et al., 2000). Studies of West Nile virus infection in the mouse model indicate that IP-10 is induced in neurons and promotes T-cell trafficking (Klein et al., 2005; Zhang et al., 2008). CXCR3, the receptor for IP-10, is one of several prominent chemokine receptors expressed in the CNS at various stages of mouse hepatitis virus (MHV)-induced encephalomyelitis (Lane et al., 2006). NDV induces the mouse homolog of IP-10 (Crg-2) in glial cells and astrocytes, while measles virus induces IP-10 in glioblastoma cells (Cheng et al., 1998; Fisher et al., 1995; Nazar et al., 1997; Vanguri and Farber, 1994). Since IP-10 by its name (interferon induced inflammatory protein) is widely known to be induced by IFN-γ, our detection of increased levels of IP-10 in NiV infected endothelial cells was somewhat unexpected, as IFN-γ is primarily produced by activated T cells. However, there are other signaling pathways that do not require IFN-γ which can contribute to IP-10 expression. The HIV Tat induces IP-10 via the p38 MAP kinase pathway and to induce IL-8 and MCP-1 via the ERK1/2 pathway (Kutsch et al., 2000). The MAP kinase and ERK1/2 pathways have not yet been examined as potential players in the pathogenesis of NiV infection. The finding that RIG-I mediated induction of IFN-β and activation of dendritic cells requires an intact p38 MAP kinase pathway emphasizes the need for the investigation of these respective signaling pathways (Mikkelsen et al., 2009). Another important if not overlooked area of study is the impact of NiV induced chemokines on the action of matrix metalloproteinases in the CNS (Khuth et al., 2001; Owens et al., 2005). It is notable that even though we have correlated upregulated inflammatory chemokine levels with increased monocyte and T-lymphocyte chemotaxis, incubating NiV infected supernatants with antibodies against IL-8 and MCP-1 simultaneously and against IP-10 individually did not ablate the increased levels of chemotaxis (data not shown). This indicates that there are other inflammatory chemokines involved that were not addressed in this study. Future studies will focus on identification of specific

chemokines crucial to inducing increased levels of monocyte and T-lymphocyte chemotaxis.

In summary, we have characterized the replication rates of NiV infection in neuronal and endothelial cells, detected antiviral responses which correlated with an unexpected cytoplasmic subcellular localization of the NiV W protein, and have characterized the innate inflammatory response of endothelial cells to NiV infection. Our findings suggest that the induction of pro-inflammatory chemokines in NiV infected primary endothelial cells *in vitro* is consistent with the observed prominent vasculitis seen in human cases of NiV infection, and these results provide initial molecular insights into the pathogenesis of NiV in humans.

Materials and methods

Cells and viruses

Primary human umbilical cord vein endothelial cells (HUVEC), human lymphatic lung microvascular endothelial cells (LYMEC), and human lung microvascular endothelial cells (HULEC) were obtained from Lonza. HUVECs were maintained according to the manufacturer's instructions in endothelial basal media (EBM) supplemented with aliquots of bovine brain extract with heparin, human epidermal growth factor, hydrocortisone, fetal bovine serum (FBS) (up to 2% final volume) and antibiotics Amphotericin B and Gentamicin, all of which were supplied by Lonza. LYMECs and HULECs were maintained in EBM-2 (Lonza) supplemented with aliquots of human epidermal growth factor, vascular endothelial growth factor, fibroblast growth factor, insulin-like growth factor, FBS (up to 5% final volume), hydrocortisone, and antibiotics Amphotericin B and Gentamicin all provided by Lonza. Endothelial cells obtained from Lonza were used within the first 5 passages, and were cultured in flasks pre-treated with 0.1% gelatin (Sigma). An immortalized human brain endothelial cell line (HBEC) was obtained from the Cell Culture Development Team at CDC, and was used within passage numbers 8–15. HBECs and EA926.hy cells (hybrid fusion of HUVEC and A549 cells) (ATCC) were maintained in M199 medium supplemented with 15% fetal bovine serum (FBS) (GIBCO-BRL Life Technologies, Inc., Frederick, MD), 16 U/mL heparin (ESI Pharmaceuticals, Cherry Hill, NJ), 25 mM HEPES buffer, 2 mM L-glutamine, 100 U/mL penicillin, and 100 U/mL streptomycin. BE(2)-M17 human neuroblastoma cells (M17) were obtained from ATCC and maintained in OPTI-MEM supplemented with 5% FBS. THP-1 monocytic leukemia cells and Jurkat JE-6.1 cells (ATCC TB-152) were maintained in RPMI 1640 with 10% FBS, 100 U/mL penicillin and 100 U/mL streptomycin. Vero and A549 cells were maintained in DMEM with 10% FBS, 100 U/mL penicillin and 100 U/mL streptomycin. All cell lines were cultured at 37 °C with 5% CO_2. All work with live NiV was performed under biosafety level 4 conditions in the Maximum Containment Laboratory (MCL) at the Centers for Disease Control and Prevention or at the Australian Animal Health Laboratory (AAHL). The NiV stock used in these experiments were from an isolate from the Malaysian outbreak in 1999 (Chua et al., 2000), passed four times on Vero E6 cells. Any potentially infectious material removed from the MCL was either sterilized with 5×10^6 rad in a Cobalt-60 gamma cell irradiator or chemically denatured with TRIZOL reagent (Invitrogen). Encephalomyocarditis virus (EMCV) was propagated in HeLa cells and had a titer of ~4.95×10^5 $TCID_{50}$/mL.

NiV immunolabeling assay

Assays were performed as previously described (Aljofan et al., 2008). Briefly, 96-well white plates of NiV infected endothelial and neuronal cells fixed with 100% cold methanol 16 h post-infection were washed 3 times with Phosphate Buffered Saline containing 0.05% Tween-20 (PBS-T). Plates then were protein blocked with 100 mL of 2% skim milk in PBS-T and incubated at 37 °C for 30 min. After protein blocking, plates were washed 3 times with PBS-T, followed by incubation with 100 μL anti-NiV antibody (prepared by AAHL's Bioreagents Development Group) diluted 1:1000 in PBS-T containing 2% skim milk for 30 min at 37 °C and then washed 3 times with PBS-T. Plates were incubated with 1% H_2O_2 (Sigma) for 15 min at room temperature then washed with PBS-T 3 times. Anti-rabbit HRP conjugated antibody 100 μL (Sigma) diluted 1:2000 in PBS-T containing 2% skim milk, were added to each well and plates incubated at 37 °C for 30 min. Plates were washed 3 times with PBS-T and 100 μL aliquots of Chemiluminescent Peroxidase Substrate-3 (CPS-3, Sigma) diluted 1:10 in Chemiluminescent assay buffer (20 mM Tris–HCl, 1 mM $MgCl_2$, pH 9.6) were added to all wells. Plates were incubated at room temperature for approximately 15 min, and then read using a Luminoskan Ascent luminometer (Thermo) using 100 ms integration per well.

Immunofluorescence assay

~5×10^3 neuronal or endothelial cells were seeded onto 8-chamber glass slides pre-treated with 0.1% gelatin (for endothelial cells), and infected with NiV at multiplicity of infection (MOI) of 0.1 (for M17) to 1 (endothelial cells). After 16–48 h, slides were fixed with cold methanol for 15 min, and upon removal of the methanol, were allowed to dry at room temperature before either being stored at −20 °C or blocked with blocking buffer (PBS, 0.1% Triton X-100, 10% goat serum) for 5–10 min. Primary antibodies generated against NiV W (Lo et al., 2009) was diluted in blocking buffer at a dilution of 1:500, then added to the chamber slides which were incubated at room temperature for 45 min. After 3 washes with blocking buffer, slides were incubated with a secondary goat anti-mouse antibody conjugated with FITC diluted 1:1000 in blocking buffer, along with a 1:1000 dilution of DAPI to stain the nuclei. Slides were viewed on an AxioScope microscope, and AxioVision version 4.7 was used to capture images (Zeiss).

One-step growth curve/median tissue culture infectious dose ($TCID_{50}$) analysis

Briefly, 5×10^4 to 4.5×10^5 cells were seeded on 6-well plates and infected for 1 h at a multiplicity of infection (MOI) of 1 or 2. Inoculum was removed and replaced with 2 mL of fresh media per well. Supernatants of infected cells were collected at 2, 5, 8, 16, 24, 48, and 64 h post-infection and were serially diluted ten-fold to infect ~3–4×10^4 Vero cells in a 96-well plate to determine the $TCID_{50}$/mL, which was calculated using the Spearman–Kärber method (Kärber, 1931). To generate IFN-β control supernatants, endothelial cells were treated with 50 mg/mL of polyinosinic:polycytidylic acid (poly-I:C) for 24 h before the supernatants were harvested and gamma-irradiated as mentioned above.

Luminex® multiplex cytokine bead assay

100 μL of gamma-irradiated supernatant per sample was subjected to a Luminex multiplex cytokine bead assay according to manufacturer's protocols (Invitrogen). Briefly, supernatants were incubated for 2 h in a 96-well filter plate with a mixture of beads conjugated with antibodies specific for Interleukin 6 (IL-6), (IL-8/CXCL8), IL-1β, inflammatory protein 10 (IP-10/CXCL 10), and monocyte chemoattractant protein 1 (MCP-1/CCL2). After two washes, the beads were incubated for 1 h with biotinylated detector antibodies specific for different epitopes of aforementioned cytokines and chemokines. After another two washes, the beads were incubated with streptavidin conjugated with phycoerythrin (PE) for 30 min. After 3 washes, the beads were resuspended in 100 μL of wash buffer, and the fluorescence signal of the PE was read in the xMap® System using a Luminex® 100 IS cytometer (Bio-Rad). Levels of cytokines present in

the samples were measured using cytokine standards provided with the bead kits (Invitrogen).

RNA extraction, reverse transcription, and real-time PCR

Total RNA were extracted from infected cell lysates using TRIZOL reagent (Invitrogen). 0.5 to 1 μg of RNA from each sample was treated with DNase I (Invitrogen), and subject to reverse transcription with oligo-dT_{12-18} primers (Invitrogen) using Superscript III reverse transcriptase (Invitrogen). The resulting cDNA was diluted 1 in 5, from which 2 μL of cDNA was used in a 25 μL real-time PCR reaction using cytokine gene-specific primers with the Jumpstart SYBR Green kit (Sigma) on an ABI 7900HT PRISM sequence detection system (Applied Biosystems). Primer sequences of specific cytokine genes are available upon request. To determine the number of NiV N gene copies present in infected cell lysates (5 h post-infection), RNA extraction and reverse transcription was performed as stated above with a primer which anneals to the 3′ end of the genome. Ensuing real-time PCR was performed as above using primers targeting the NiV N gene. NiV N gene copy numbers were calculated using a standard curve generated by 10-fold dilutions of a predetermined copy number of synthetic NiV N gene RNA.

Interferon bioassay

Assays were performed as described previously with some modifications (Green et al., 1980). Briefly, 3.5×10^4 A549 cells per well were plated in 96-well microtiter plates. Cells were treated for 6 h with either interferon beta (IFN-β) (Invitrogen), or 100 μL of gamma-irradiated supernatants from cells infected with NiV. Supernatants were removed, and each well was infected with ~200 PFU of Encephalomyocarditis virus (EMCV) for 16–20 h in DMEM supplemented with 10% FBS. The supernatants were then removed, and the cells were stained with crystal violet solution for 5 min, washed once with PBS, and were scored for cytopathic effect (CPE) using a TECAN Sunrise plate reader at an absorbance of 600 nm. Uninfected cells stained with crystal violet served as a negative control for levels of CPE and was scored as having 100% protection from EMCV-induced CPE.

Interferon-β ELISA

Assays were performed according to manufacturer's protocols using a one-step sandwich human IFN-β ELISA kit (Invitrogen). Briefly, 100 μL of gamma-irradiated supernatants from NiV infected cells were added to each well of a 96-well microplate pre-coated with affinity-purified polyclonal antibody to human IFN-β, along with 50 μL of horseradish peroxidase labeled-antibody for 2 h on a plate shaker. After 3 washes, 100 μL of color developing solution was added to each well and incubated at room temperature for 30 min, upon which 100 μL of reaction stopper solution was added to each well. The absorbance of the reaction mixture in each well was read at 450 nm, with the reference wavelength set to 630 nm.

Chemotaxis assay

Assays were performed according to manufacturer's instructions using the Chemicon QCM™ 5 μm 96-well cell migration kit (Millipore). In brief, THP-1 or JE-6.1 cells were centrifuged (1500 RPM, 5 min), resuspended to a cell count of $\sim1.5\times10^6$/mL, and starved in DMEM without serum or chemoattractants for ~2 h before being resuspended in fresh media and dispensed into the migration chamber at $1.2–1.5\times10^5$/well. Wells of a 96-well feeder tray were filled with 150 μL of either fresh endothelial growth media, or gamma-irradiated supernatants from NiV infected cells. After a 2 h incubation of the chambers in the feeder wells, transmigrated cells in the feeder wells were transferred to a 96-well plate, while transmigrated cells attached to the outer surface of the incubation chamber were washed into a new feeder plate. These detached cells were then combined with the transmigrated cells in the 96-well plate, which were lysed with a lysis buffer mixed with CyQuant GR Dye, which is a DNA-binding fluorescent dye. The cell lysates were then transferred to white microtiter plates (Thermo) and read with a Fluoroskan Ascent fluorescence plate reader using the 480/520 nm filter set (Thermo) with an integration time of 120 ms. Fluorescence levels of the DNA-binding dye present in the cell lysates were indicative of the relative number of cells that migrated through the chamber. Supernatants taken from poly-I:C stimulated endothelial cells served as positive controls for maximum induction of transmembrane migration of THP-1 cells.

Statistical methods

The immunolabeling assay, IFN-β ELISA, EMCV CPE assay, quantitative cytokine and chemokine mRNA and protein expression profiles, and chemotaxis assays were compared using two-tailed Student's *t*-tests with Welch's modification. Differences were considered significant at $P<0.05$.

Acknowledgments

MKL was supported by funding from Oak Ridge Institute for Science and Education. MA was supported by a CSIRO, OCE PhD scholarship. DM was supported by funding from Battelle National Biodefense Institute, Frederick, MD, USA.

Appendix A. Supplementary data

Supplementary data associated with this article can be found, in the online version, at doi:10.1016/j.virol.2010.05.005.

References

Aljofan, M., Porotto, M., Moscona, A., Mungall, B.A., 2008. Development and validation of a chemiluminescent immunodetection assay amenable to high throughput screening of antiviral drugs for Nipah and Hendra virus. J. Virol. Methods 149 (1), 12–19.

Antony, V.B., Godbey, S.W., Kunkel, S.L., Hott, J.W., Hartman, D.L., Burdick, M.D., Strieter, R.M., 1993. Recruitment of inflammatory cells to the pleural space. Chemotactic cytokines, IL-8, and monocyte chemotactic peptide-1 in human pleural fluids. J. Immunol. 151 (12), 7216–7223.

Cheng, G., Nazar, A.S., Shin, H.S., Vanguri, P., Shin, M.L., 1998. IP-10 gene transcription by virus in astrocytes requires cooperation of ISRE with adjacent kappaB site but not IRF-1 or viral transcription. J. Interferon Cytokine Res. 18 (11), 987–997.

Childs, K., Stock, N., Ross, C., Andrejeva, J., Hilton, L., Skinner, M., Randall, R., Goodbourn, S., 2007. mda-5, but not RIG-I, is a common target for paramyxovirus V proteins. Virology 359 (1), 190–200.

Childs, K.S., Andrejeva, J., Randall, R.E., Goodbourn, S., 2009. Mechanism of mda-5 Inhibition by paramyxovirus V proteins. J. Virol. 83 (3), 1465–1473.

Chua, K.B., Bellini, W.J., Rota, P.A., Harcourt, B.H., Tamin, A., Lam, S.K., Ksiazek, T.G., Rollin, P.E., Zaki, S.R., Shieh, W., Goldsmith, C.S., Gubler, D.J., Roehrig, J.T., Eaton, B., Gould, A.R., Olson, J., Field, H., Daniels, P., Ling, A.E., Peters, C.J., Anderson, L.J., Mahy, B.W., 2000. Nipah virus: a recently emergent deadly paramyxovirus. Science 288 (5470), 1432–1435.

Ciancanelli, M.J., Volchkova, V.A., Shaw, M.L., Volchkov, V.E., Basler, C.F., 2009. Nipah virus sequesters inactive STAT1 in the nucleus via a P gene-encoded mechanism. J. Virol. 83 (16), 7828–7841.

Curran, J., Kolakofsky, D., 1990. Sendai virus P gene produces multiple proteins from overlapping open reading frames. Enzyme 44 (1–4), 244–249.

Emeny, J.M., Morgan, M.J., 1979. Regulation of the interferon system: evidence that Vero cells have a genetic defect in interferon production. J. Gen. Virol. 43 (1), 247–252.

Erbar, S., Diederich, S., Maisner, A., 2008. Selective receptor expression restricts Nipah virus infection of endothelial cells. Virol. J. 5, 142.

Fisher, S.N., Vanguri, P., Shin, H.S., Shin, M.L., 1995. Regulatory mechanisms of MuRantes and CRG-2 chemokine gene induction in central nervous system glial cells by virus. Brain Behav. Immun. 9 (4), 331–344.

Giorgi, C., Blumberg, B.M., Kolakofsky, D., 1983. Sendai virus contains overlapping genes expressed from a single mRNA. Cell 35 (3 Pt 2), 829–836.

Glabinski, A.R., Ransohoff, R.M., 1999. Chemokines and chemokine receptors in CNS pathology. J. Neurovirol. 5 (1), 3–12.

Goh, K.J., Tan, C.T., Chew, N.K., Tan, P.S., Kamarulzaman, A., Sarji, S.A., Wong, K.T., Abdullah, B.J., Chua, K.B., Lam, S.K., 2000. Clinical features of Nipah virus encephalitis among pig farmers in Malaysia. N. Engl. J. Med. 342 (17), 1229–1235.
Gotoh, B., Komatsu, T., Takeuchi, K., Yokoo, J., 2002. Paramyxovirus strategies for evading the interferon response. Rev. Med. Virol. 12 (6), 337–357.
Green, J.A., Yeh, T.J., Overall Jr., J.C., 1980. Rapid, quantitative, semiautomated assay for virus-induced and immune human interferons. J. Clin. Microbiol. 12 (3), 433–438.
Griffin, D.E., 1997. Cytokines in the brain during viral infection: clues to HIV-associated dementia. J. Clin. Invest. 100 (12), 2948–2951.
Horvath, C.M., 2004. Silencing STATs: lessons from paramyxovirus interferon evasion. Cytokine Growth Factor Rev. 15 (2–3), 117–127.
Hossain, M.J., Gurley, E.S., Montgomery, J.M., Bell, M., Carroll, D.S., Hsu, V.P., Formenty, P., Croisier, A., Bertherat, E., Faiz, M.A., Azad, A.K., Islam, R., Molla, M.A., Ksiazek, T.G., Rota, P.A., Comer, J.A., Rollin, P.E., Luby, S.P., Breiman, R.F., 2008. Clinical presentation of nipah virus infection in Bangladesh. Clin. Infect. Dis. 46 (7), 977–984.
Kärber, G., 1931. Beitrag zur kollektiven Behandlung pharmakologischer Reihenversuche. Arch. Exp. Pathol. Pharmakol. 162, 480–483.
Khuth, S.T., Akaoka, H., Pagenstecher, A., Verlaeten, O., Belin, M.F., Giraudon, P., Bernard, A., 2001. Morbillivirus infection of the mouse central nervous system induces region-specific upregulation of MMPs and TIMPs correlated to inflammatory cytokine expression. J. Virol. 75 (17), 8268–8282.
Klein, R.S., 2004. Regulation of neuroinflammation: the role of CXCL10 in lymphocyte infiltration during autoimmune encephalomyelitis. J. Cell. Biochem. 92 (2), 213–222.
Klein, R.S., Lin, E., Zhang, B., Luster, A.D., Tollett, J., Samuel, M.A., Engle, M., Diamond, M.S., 2005. Neuronal CXCL10 directs CD8+ T-cell recruitment and control of West Nile virus encephalitis. J. Virol. 79 (17), 11457–11466.
Kolakofsky, D., Roux, L., Garcin, D., Ruigrok, R.W., 2005. Paramyxovirus mRNA editing, the "rule of six" and error catastrophe: a hypothesis. J. Gen. Virol. 86 (Pt 7), 1869–1877.
Kulkarni, S., Volchkova, V., Basler, C.F., Palese, P., Volchkov, V.E., Shaw, M.L., 2009. Nipah virus edits its P gene at high frequency to express the V and W proteins. J. Virol. 83 (8), 3982–3987.
Kunkel, E.J., Boisvert, J., Murphy, K., Vierra, M.A., Genovese, M.C., Wardlaw, A.J., Greenberg, H.B., Hodge, M.R., Wu, L., Butcher, E.C., Campbell, J.J., 2002. Expression of the chemokine receptors CCR4, CCR5, and CXCR3 by human tissue-infiltrating lymphocytes. Am. J. Pathol. 160 (1), 347–355.
Kutsch, O., Oh, J., Nath, A., Benveniste, E.N., 2000. Induction of the chemokines interleukin-8 and IP-10 by human immunodeficiency virus type 1 tat in astrocytes. J. Virol. 74 (19), 9214–9221.
Lane, T.E., Hardison, J.L., Walsh, K.B., 2006. Functional diversity of chemokines and chemokine receptors in response to viral infection of the central nervous system. Curr. Top. Microbiol. Immunol. 303, 1–27.
Lee, K.E., Umapathi, T., Tan, C.B., Tjia, H.T., Chua, T.S., Oh, H.M., Fock, K.M., Kurup, A., Das, A., Tan, A.K., Lee, W.L., 1999. The neurological manifestations of Nipah virus encephalitis, a novel paramyxovirus. Ann. Neurol. 46 (3), 428–432.
Liston, P., Briedis, D.J., 1995. Ribosomal frameshifting during translation of measles virus P protein mRNA is capable of directing synthesis of a unique protein. J. Virol. 69 (11), 6742–6750.
Lo, M.K., Harcourt, B.H., Mungall, B.A., Tamin, A., Peeples, M.E., Bellini, W.J., Rota, P.A., 2009. Determination of the henipavirus phosphoprotein gene mRNA editing frequencies and detection of the C, V and W proteins of Nipah virus in virus-infected cells. J. Gen. Virol. 90 (Pt 2), 398–404.
Loetscher, P., Seitz, M., Clark-Lewis, I., Baggiolini, M., Moser, B., 1994. Monocyte chemotactic proteins MCP-1, MCP-2, and MCP-3 are major attractants for human CD4+ and CD8+ T lymphocytes. FASEB J. 8 (13), 1055–1060.
Mahalingam, S., Farber, J.M., Karupiah, G., 1999. The interferon-inducible chemokines MuMig and Crg-2 exhibit antiviral activity In vivo. J. Virol. 73 (2), 1479–1491.
Manuse, M.J., Parks, G.D., 2009. Role for the paramyxovirus genomic promoter in limiting host cell antiviral responses and cell killing. J. Virol. 83 (18), 9057–9067.
Mayo, M.A., 2002. A summary of taxonomic changes recently approved by ICTV. Arch. Virol. 147 (8), 1655–1663.
Melchjorsen, J., Jensen, S.B., Malmgaard, L., Rasmussen, S.B., Weber, F., Bowie, A.G., Matikainen, S., Paludan, S.R., 2005. Activation of innate defense against a paramyxovirus is mediated by RIG-I and TLR7 and TLR8 in a cell-type-specific manner. J. Virol. 79 (20), 12944–12951.
Mikkelsen, S.S., Jensen, S.B., Chiliveru, S., Melchjorsen, J., Julkunen, I., Gaestel, M., Arthur, J.S., Flavell, R.A., Ghosh, S., Paludan, S.R., 2009. RIG-I-mediated activation of p38 MAPK is essential for viral induction of interferon and activation of dendritic cells: dependence on TRAF2 and TAK1. J. Biol. Chem. 284 (16), 10774–10782.
Nazar, A.S., Cheng, G., Shin, H.S., Brothers, P.N., Dhib-Jalbut, S., Shin, M.L., Vanguri, P., 1997. Induction of IP-10 chemokine promoter by measles virus: comparison with interferon-gamma shows the use of the same response element but with differential DNA-protein binding profiles. J. Neuroimmunol. 77 (1), 116–127.
Owens, T., Babcock, A.A., Millward, J.M., Toft-Hansen, H., 2005. Cytokine and chemokine inter-regulation in the inflamed or injured CNS. Brain Res. Brain Res. Rev. 48 (2), 178–184.
Pace, E., Gjomarkaj, M., Melis, M., Profita, M., Spatafora, M., Vignola, A.M., Bonsignore, G., Mody, C.H., 1999. Interleukin-8 induces lymphocyte chemotaxis into the pleural space. Role of pleural macrophages. Am J Respir Crit Care Med 159 (5 Pt 1), 1592–1599.
Parisien, J.P., Bamming, D., Komuro, A., Ramachandran, A., Rodriguez, J.J., Barber, G., Wojahn, R.D., Horvath, C.M., 2009. A shared interface mediates paramyxovirus interference with antiviral RNA helicases MDA5 and LGP2. J. Virol. 83 (14), 7252–7260.
Park, M.S., Shaw, M.L., Munoz-Jordan, J., Cros, J.F., Nakaya, T., Bouvier, N., Palese, P., Garcia-Sastre, A., Basler, C.F., 2003. Newcastle disease virus (NDV)-based assay demonstrates interferon-antagonist activity for the NDV V protein and the Nipah virus V, W, and C proteins. J. Virol. 77 (2), 1501–1511.
Paton, N.I., Leo, Y.S., Zaki, S.R., Auchus, A.P., Lee, K.E., Ling, A.E., Chew, S.K., Ang, B., Rollin, P.E., Umapathi, T., Sng, I., Lee, C.C., Lim, E., Ksiazek, T.G., 1999. Outbreak of Nipah-virus infection among abattoir workers in Singapore. Lancet 354 (9186), 1253–1256.
Penido, C., Vieira-de-Abreu, A., Bozza, M.T., Castro-Faria-Neto, H.C., Bozza, P.T., 2003. Role of monocyte chemotactic protein-1/CC chemokine ligand 2 on gamma delta T lymphocyte trafficking during inflammation induced by lipopolysaccharide or Mycobacterium bovis bacille Calmette-Guerin. J. Immunol. 171 (12), 6788–6794.
Plumet, S., Herschke, F., Bourhis, J.M., Valentin, H., Longhi, S., Gerlier, D., 2007. Cytosolic 5′-triphosphate ended viral leader transcript of measles virus as activator of the RIG I-mediated interferon response. PLoS ONE 2 (3), e279.
Rodriguez, J.J., Parisien, J.P., Horvath, C.M., 2002. Nipah virus V protein evades alpha and gamma interferons by preventing STAT1 and STAT2 activation and nuclear accumulation. J. Virol. 76 (22), 11476–11483.
Rodriguez, J.J., Cruz, C.D., Horvath, C.M., 2004. Identification of the nuclear export signal and STAT-binding domains of the Nipah virus V protein reveals mechanisms underlying interferon evasion. J. Virol. 78 (10), 5358–5367.
Shaw, M.L., Garcia-Sastre, A., Palese, P., Basler, C.F., 2004. Nipah virus V and W proteins have a common STAT1-binding domain yet inhibit STAT1 activation from the cytoplasmic and nuclear compartments, respectively. J. Virol. 78 (11), 5633–5641.
Shaw, M.L., Cardenas, W.B., Zamarin, D., Palese, P., Basler, C.F., 2005. Nuclear localization of the Nipah virus W protein allows for inhibition of both virus- and toll-like receptor 3-triggered signaling pathways. J. Virol. 79 (10), 6078–6088.
Shingai, M., Ebihara, T., Begum, N.A., Kato, A., Honma, T., Matsumoto, K., Saito, H., Ogura, H., Matsumoto, M., Seya, T., 2007. Differential type I IFN-inducing abilities of wild-type versus vaccine strains of measles virus. J. Immunol. 179 (9), 6123–6133.
Singh, A., Kulshreshtha, R., Mathur, A., 2000. Secretion of the chemokine interleukin-8 during Japanese encephalitis virus infection. J. Med. Microbiol. 49 (7), 607–612.
Stamatovic, S.M., Shakui, P., Keep, R.F., Moore, B.B., Kunkel, S.L., Van Rooijen, N., Andjelkovic, A.V., 2005. Monocyte chemoattractant protein-1 regulation of blood–brain barrier permeability. J. Cereb. Blood Flow Metab. 25 (5), 593–606.
Vanguri, P., Farber, J.M., 1994. IFN and virus-inducible expression of an immediate early gene, crg-2/IP-10, and a delayed gene, I-A alpha in astrocytes and microglia. J. Immunol. 152 (3), 1411–1418.
Wong, K.T., Shieh, W.J., Kumar, S., Norain, K., Abdullah, W., Guarner, J., Goldsmith, C.S., Chua, K.B., Lam, S.K., Tan, C.T., Goh, K.J., Chong, H.T., Jusoh, R., Rollin, P.E., Ksiazek, T. G., Zaki, S.R., 2002. Nipah virus infection: pathology and pathogenesis of an emerging paramyxoviral zoonosis. Am. J. Pathol. 161 (6), 2153–2167.
Zhang, Y., Luxon, B.A., Casola, A., Garofalo, R.P., Jamaluddin, M., Brasier, A.R., 2001. Expression of respiratory syncytial virus-induced chemokine gene networks in lower airway epithelial cells revealed by cDNA microarrays. J. Virol. 75 (19), 9044–9058.
Zhang, B., Chan, Y.K., Lu, B., Diamond, M.S., Klein, R.S., 2008. CXCR3 mediates region-specific antiviral T cell trafficking within the central nervous system during West Nile virus encephalitis. J. Immunol. 180 (4), 2641–2649.